Electrochimica Acta 293 (2019) 25–29

Contents lists available at ScienceDirect

Electrochimica Acta

journal homepage: www.elsevier.com/locate/electacta

Composite electrolytes of pyrrolidone-derivatives-PEO enable to enhance performance of all solid state lithium-ion batteries

Xin Li [a], Zijian Wang [a], Hai Lin [a], Yidong Liu [a, **], Yong Min [b], Feng Pan [a, *]

[a] School of Advanced Materials, Peking University Shenzhen Graduate School, Shenzhen, 518055, China
[b] School of Materials and Energy, Guangdong University of Technology, Guangzhou, 510006, China

ARTICLE INFO

Article history:
Received 12 July 2018
Received in revised form
4 October 2018
Accepted 4 October 2018
Available online 5 October 2018

Keywords:
Li ion battery
Solid state
Composite electrolytes
Pyrrolidone derivatives
High ambient conductivity

ABSTRACT

All-solid-state batteries with $LiFePO_4$ cathodes and polyethylene oxide (PEO) based electrolytes are optimized with organic polymer synthesized from allyl amine and tartaric acid which show better properties including ionic conductivity, electrochemical window, charge-discharge capacity and rate performance. The rate of PEO ($\overline{MW}$ = 4,000,000) and lithium salt (Lithium bis(trifluoromethanesulphonyl)imide, LiTFSI) is 75:20 (w/w) and polymers of different molecular weight are tested at a wide temperature range from 27 °C (ambient temperature) to 120 °C. Electrolytes with larger amount (weighting more than half of PEO) of low-molecular-weight polymer show conductivity of above 10^{-4} S cm^{-1}, which is similar to typical gel-polymer-electrolyte. Electrolytes made of high-molecular-weight dopant, PEO and LiTFSI through ball milling show better conductivity (5.4×10^{-6} S cm^{-1}) as well as better strength than electrolytes without dopant (1.3×10^{-6} S cm^{-1}) at room temperature. And a sensitive dependence on temperature increasing is also observed constructing to the sample without dopant. Stability below 120 °C also indicates promising use of this composite electrolyte in solid state lithium ion batteries.

1. Introduction

Due to its significant development in recent years, lithium ion batteries have participated in many fields of our daily life and production, such as electronic equipment, electric vehicles and energy stowage of power plants [1–4]. As the key part of a battery, gel or liquid electrolytes could cause safety problems because of the heat and flammable gas release. Solid state electrolytes (SSE) could keep out of these safety problems and dendrite of Li. Besides, batteries with SSE have higher theoretical energy density, which makes it the hotpot of battery researches these years [5–7]. However, problems such as poor room conductivity, narrow electrochemical window, large interfacial and grain boundary resistance still remain to be solved [8–11]. Boronized polyethylene glycol with inorganic particles and metal-organic-framework have been used to make differences in electrodes compatibilities, interfacial resistances and polarization effects [12,13]. And plenty of works concentrated to the modification of cathode materials with nanofiber networks and particles based on PEO-SSE has been reported [14,15].

PEO has been considered as the most promising solid polymer electrolyte substrate since it was reported [3,16]. Although it has poor ionic conductivity, plenty of O atoms with lone pair electrons make it easy to coordinate with Li and other atoms, resulting to the possibility of improving ionic conductivity through the adding of lithium salts and inorganic particles [17]. Plasticizers can also promote dissociation of ions thus exhibit ionic conductivity under suitable concertation before dielectric constants increase [18–21]. Own to the segmental motion of PEO chains and ionic motion of Li^+, amorphous complexes can provide good conductivity [22,23]. A lot of study has been performed to improve the ionic conductivity of PEO based solid polymer electrolytes through the co-polymerization, branching, doping and many other ways [24–27].

Tartaric acid and amines could react to synthesis pyrrolidone derivates with −OH groups, which are supposed to be of good compatibility with PEO while lower its degree of crystallinity [28,29]. We use allyl amine hydrochloride for its polymer is easy to purchase at low price as a widely used product. And as a polymer composite, the new electrolyte would not change too much in process ability. Various classes of electrolytes are prepared through

* Corresponding author.
** Corresponding author.
E-mail addresses: liuyd@pkusz.edu.cn (Y. Liu), panfeng@pkusz.edu.cn (F. Pan).

https://doi.org/10.1016/j.electacta.2018.10.023
0013-4686/

pyrrolidone derivates doping and influences of the dopants to the conductivity of PEO-LiTFSI system were studied through electrochemical impedance spectroscopy (EIS) in this work. As the amount of low-molecular-weight dopant increasing, the strength of the composite electrolytes decreases and conductivity performance is close to gel electrolytes (over 10^{-4} S cm^{-1} at room temperature [3]). Large-molecule-weight dopant increases the strength of PEO and makes a difference in conductivity. Differential scanning calorimetry (DSC) curves and thermal gravimetric analyzer (TGA) indicate good stability below 120 °C and infrared spectroscopies (IR) of the electrolyte films and its components are also analyzed.

2. Experimental section

2.1. Apparatus and reagent

A ball milling instrument (Retsch PM200) was used to mix up solid complexes. Electrochemical impedance spectroscopy (ESI) and LSV was performed with an electrochemical workstation of Shanghai Chenhua (CHI604E and its Software) and the data were further processed and graphed with Origin Software. DSC and TGA test was performed with an instrument of Mettler Toledo (TGA/DSC1).

Infrared spectroscopy was identified with Frontier FT-IR Spectrometer (PerkinElmer).

L- (+)-tartaric acid (99+%) was purchased from Acros. LiTFSI was purchased from Adamas. PEO ($\overline{MW}$ = 4,000,000) and acetylene black were purchased from the Dow chemical company. Acetonitrile (99%), trimethylamine (99.5%), 4-dimethylaminopyridine (DMAP), 1-ethyl-3-(3-dimethylaminopropyl) carbodiimide hydrochloride (EDC·HCl), pyridine (99.5%), ammonium persulfate (98%), N-Methyl pyrrolidone (NMP, 99%) and Poly (vinylidene fluoride) (PVDF) were purchased from InnoChem. Poly (allyl amine hydrochloride (PAA·HCl) ($\overline{MW}$ = 12000–20000) was purchased from Sigma-Aldrich. Allyl amine hydrochloride (98%) was purchased from TCI. Carbon-coated $LiFePO_4$ (LFP) was purchased from Dynanonic.

Commercial purified water was purged with a Milli-Q Advantage system before using.

2.2. Electrolytes procedure

2.2.1. Low-molecular-weight dopant synthesize

10 mmol of allylamine hydrochloride was dissolved in 20 mL water under nitrogen atmosphere; 6 mol% of ammonium persulfate dissolved in 10 mL water was added dropwise in 3 h at 90 °C. The solution was subsequently stirred under nitrogen atmosphere at 90 °C for 4 h. Then the mixture was poured into excess methanol and filtered with Buchner funnel [19]. After dried under vacuum for 24 h, the PAA·HCl was mixed with 2 eq. (to the monomer) trimethylamine, 2 eq. DMAP, 2 eq. EDC·HCl and 40 mL water; 1.3 eq. L-(+)-tartaric acid dissolved in 20 mL water was added dropwise under stirring [30–32]. White solid precipitated and dissolved very fast under stirring at the very beginning. Then yellow cotton-shaped solid appeared and gathered at the bottom of three-neck-flask. The mixture was stirred overnight and liquid phase was poured while the yellow solid washed with 10 mL water for 3 times and then freeze-dried under vacuum for 24 h.

2.2.2. High-molecular-weight dopant synthesize

High-molecular-weight PAA·HCl ($\overline{MW}$ = 12000–20000) was purchased from Sigma-Aldrich and the reaction with tartaric acid was conducted in the same process with low-molecular PAA.

PEO and LiTFSI were mixed in a rate of 75:20 (w/w) and then various amount of the organic dopant was added. Electrolytes with low-molecular dopant were dissolved in acetonitrile and stirred at 80 °C in a glove box for 3 days and then dropped onto a Teflon plate. The Teflon plate with mixture drops was put into a vacuum oven heating to 60 °C for 5 days to move out the acetonitrile. Electrolytes with high-molecular dopant could not totally dissolve in general solvents. To mix the complexes, a sealed ball mill with ZrO_2 balls was used. Solid mixture harder than PEO was gained after milling for 8 h at 400 r min^{-1}.

LFP, PVDF and acetylene black (5:3:2, w/w/w) were mixed in NMP and stirred overnight. Then the slurry was coating to a stainless steel foil. After dried at 80 °C for 12 h, it was cut and used as cathodes and the active material loading is around 0.4 mg cm^{-2}.

2.3. Methods

Electrolytes were put between two blocking electrodes and packed up in steel button cells under pressure of 10 MPa for further test. Conductivity measurement was conducted with AC impedance with frequency ranged from 0.01 Hz to 1 MHz and a perturbation voltage of 10 mV AC amplitude at different temperatures. Pre-activation was processed and the materials were tested several times at each temperature to insure the stability and reliability.

The electrochemical stability window of the prepared electrolytes was determined with Chenhua electrochemical workstation in a three electrode system where a stainless steel blocking electrode was used as a working electrode and lithium metal foil as both reference and counter electrode.

TGA/DSC measurement was carried out under N_2 atmosphere with a healing rate of 10 °C/min. Infrared spectroscopy and other measurements were obtained as well.

3. Result and discussion

The films of electrolytes with low-molecular-weight dopant whose rate of dopant and PEO (w/w) ranged from 4:1: to 0.5:1 is too weak to separate two blocking electrodes, so nylon gasket (16*8*1.5 mm) is setting between two stainless steel plates and the electrolyte is filled into the middle. After activating for 8 h at 100 °C, AC impedance is performed (Fig. 1).

Typical low-frequency spike and high-frequency semicircle can be observed and the resistive component of the electrolytes R_b is measured upon their meeting point on the real axis. Conductivity

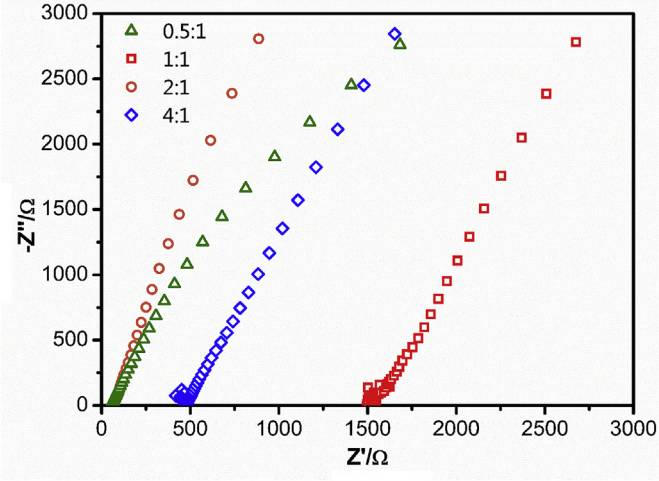

Fig. 1. Nyquist plots of electrolytes with low-molecular-weight dopant at room temperature (27 °C). The rates of PEO: LiTFSI (w/w) is 75:20 and the rate of dopant: PEO are 0.5:1, 1:1, 2:1 and 4:1, respectively.

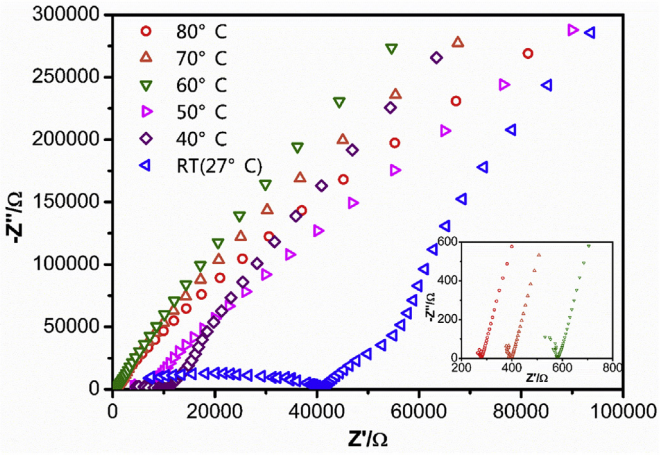

Fig. 2. Nyquist plots of electrolytes with high-molecular-weight dopant temperature ranged from room temperature (RT) to 80 °C. The rate of dopant: PEO: LiTFSI (w/w) is 5:75:20.

could be calculated from $\sigma = 4L/(\pi D^2 R_b)$, where L and D represent the thickness and diameter of the electrolytes [33].

The conductivities of these complexes are between 10^{-2} S cm^{-1} and 10^{-4} S cm^{-1} at room temperature, which are much higher than PEO-LiTFSI without doping. No obvious relationship between conductivity and doping amount is observed, which means too much dopant might have been added.

When the rate of dopant and PEO comes to 0.4:1 and below, thin films could be lifted off the Teflon plate. The films are clipped between two stainless steel plates and pressed to insure good touch with electrodes. The thickness of films is about 50 μm after pressing. AC impedance is performed after activating of 8 h at 100 °C. The Nyquist plots shows small R_b while thickness of the electrolyte films is even smaller, resulting in conductivity of about 10^{-6} S cm^{-1}. A blank sample without dopant whose rate of PEO: LiTFSI is 75: 20 (w/w) is also tested (Fig. S1). However, R_b of the blank sample is close to those doped with dopant, which means small amount dopant could hardly make a difference to the conductivity.

The conductivity at higher temperature is also measured. The conductivity increased about 20 times from room temperature to 60 °C, but this performance is still close to the blank sample (Fig. S2).

The electrolytes with high-molecular-weight dopant are pressed into films of 2.5 mm with carbon aluminum foil on both sides. Conductivity measurement is carried out after activating of 8 h at 100 °C (Fig. S3). Compared to PEO films, this complex films have better strength and remain flexible.

Fig. 2 shows the impedance plots of electrolytes whose doping rate is 5:75:20 (dopant: PEO: LiTFSI, w/w/w). The conductivities of all electrolytes calculated from R_b are showed in Table 1. The R_b increases nearly 150 times when temperature ranged from 27 °C to 80 °C, resulting in obvious increase of conductivity. Fig. S4 shows the conductivity changing of the doping sample and blank sample when the temperature ranges from 27 °C to 80 °C. In spite of lower salt concentration to blank group, the doping sample shows better beginning conductivity, which indicates that the dopant can optimize the transfer of ions. The plots of log(σ) versus T^{-1} shows two regions with different slope rate. Below the melting point of the electrolyte, the membranes contain more crystalline fraction. With the increase of temperature, the electrolyte membranes get soften and the viscosity and mobility become higher. The higher slope rate in Fig. S4 below melt point indicate that activation energy is higher than that at temperature above melting point according to the Arrhenius relation ($\sigma = \sigma_0 \exp(-E_a/k_B T)$, σ_0 is the pre-exponential factor, E_a is the activation energy, k_B is the Boltzmann constant and T is the absolute temperature). Further test at higher temperatures is obtained and the cell could work efficiently from 90 °C to 120 °C as well. These results imply promising use at room temperature and better performance when it comes to high temperature environment.

LSV between 2 V and 8 V (vs. Li/Li$^+$) of coin cells made up of Li foil anode, steel cathode and electrolyte film is obtained on Chenhua electrochemical workstation (Fig. 3). The serious current rise of doped electrolyte appears at higher potential compared to PEO-LiTFSI film. For PEO-LiTFSI (75:20, w/w) electrolyte, the rise of anodic current comes around 5.3 V vs. Li/Li$^+$ [15,34]. As for the electrolyte with dopant (5 w%), it occurs about 0.2 V higher. While the zoom in view around 4 V indicates that the composite electrolyte has been unstable obviously like other PEO-based electrolytes and the higher current rise may be caused by degradation of the dopant.

The rate capacity of the LFP/Li cells with composite electrolytes is measured in order to test the feasibility of the material. The rate of dopant/PEO/LiTFSI is 5:75:20 (w/w/w). Rate capacity and charge-discharge profiles ranging from 1C to 5C are firstly measured to trail the stability of the electrolytes films (Fig. S5). The rate capacity at 1C, 2C and 3C decreases gradually while staying above 130 mA h g^{-1}. There comes a rapid drop at rate of 4C. When it comes to 5C, the rate capacity is lower than 10 mA h g^{-1}. This capacity drop is considered to be caused by the polarization.

Then rate capacity and charge-discharge profiles of 0.2C, 0.5C, 1C, 2C, 3C and once more 0.2C are measured and the discharge capacities of the cell are 168 mA h g^{-1}, 150 mA h g^{-1}, 146 mA h g^{-1}, 141 mA h g^{-1}, 136 mA h g^{-1} and 160 mA h g^{-1}, respectively (Fig. 4). Corresponding with the formal measurement, no rapid drop occurs when rate ranges from 0.2C to 3C. Further, the discharge capacity rises to about 160 mA h g^{-1} when the rate comes back to 0.2C. These results indicate great potential of practical application in all solid lithium batteries.

Table 1
Conductivity data (S cm^{-1}) calculated from R_b.

T(°C)	Low-molecular-weight Dopant: PEO (w/w)								High-molecular-weight Dopant: PEO (w/w)			No dopant
	0.16:1	0.2:1	0.25:1	0.4:1	0.5:1	1:1	2:1	4:1	1:75	5:75	10:75	0:75
RT	4.8E-6	5.8E-6	5.5E-6	4.8E-6	5.0E-3	2.0E-4	4.0E-3	6.3E-4	4.8E-6	5.4E-6	1.6E-6	1.3E-6
40	/[a]	/	/	/	/	/	/	/	/	2.1E-5	/	4.6E-6
50	/	/	/	/	/	/	/	/	/	3.5E-5	/	2.1E-5
60	1.0E-4	4.1E-4	6.2E-5	2.5E-4	-[b]	–	–	–	2.0E-4	3.8E-4	8.4E-5	1.1E-4
70	–	–	–	–	–	–	–	–	/	5.6E-4	/	1.7E-4
80	–	–	–	–	–	–	–	–	6.1E-4	8.1E-4	2.5E-4	2.6E-4

[a] "/" stands for "not tested".
[b] "-" stands for "not stable.

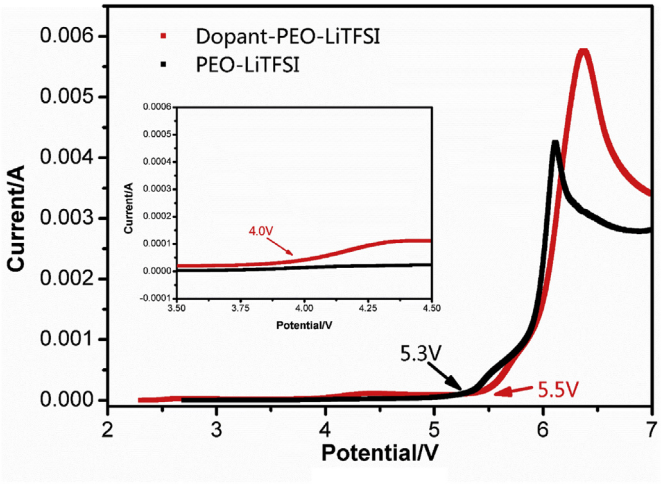

Fig. 3. LSV data of cells with PEO-LiTFSI (75:20, w/w) and dopant-PEO-LiTFSI (5:75:20, w/w) electrolyte films at 80 °C. The scan rate is 10 mV s^{-1} and quiet time is 1.8 × 10^{-3} s.

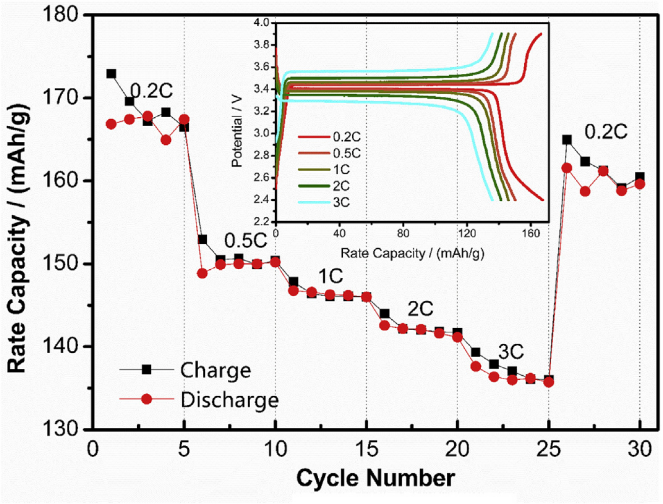

Fig. 4. Rate capacity and charge-discharge profiles of $LiFePO_4$/Li cells with electrolytes of dopant-PEO-LiTFSI (5:75:20, w/w/w) at rates of 0.2C, 0.5C, 1C, 2C, 3C and 0.2C. Temperature: 80 °C.

DSC curves of pure PEO, PEO-LiFSI (75:20, w/w), PAA·HCl, high-molecular-weight dopant and dopant-PEO-LiTFSI (5:75:20, w/w) are showed in Fig. S6. The melting point of pure PEO is 69.5 °C [35,36]. PEO-LiTFSI (75:20, w/w) has lower melting point of 61.5 °C due to the change of crystal rate of PEO [35,37]. Dopant synthesized from PAA and tartaric acid shows no resolve curve below 200 °C. Melting point of the dopant-PEO-LiTFSI electrolyte is 60.5 °C and no peak was identified before the decomposition of PEO started around 270 °C, which is accordance with the stable EIS performance under 120 °C. TGA data of composite electrolytes with low-molecular-weight dopant-PEO-LiTFSI (15:75:20) and high-molecular-weight dopant-PEO-LiTFSI (5:75:20) are showed in Fig. S7. According with the DSC data, TGA curve of electrolytes with high-molecular-weight dopant show little weight loss before 120 °C, indicating good thermodynamic stability. While electrolytes with low-molecular-weight keep losing weight from the beginning, which could be caused by water absorption from air during the preparation of DSC/TGA test and the slowly degradation of the dopant. The weight loss and DSC peak from 200 °C indicate the significant dopant degradation occurs at about 200 °C, which is more obvious in electrolyte with low-molecular-weight dopant.

The electrolyte of dopant-PEO-LiTFSI (5:75:20, w/w) is stretched into thin film for the sake of light transmission so that its infrared spectrum could be obtained (Fig. S8). Components of the complex electrolyte are also measured and displayed in Fig. 5: Films of pure PEO and PEO-LiTFSI (75:20, w/w) are obtained from removing the solvent of their acetonitrile solutions. PAA·HCl and high-molecular-weight dopant are respectively milled with KBr and performed into transparent slices for measurement. Peaks at different wave numbers and their corresponding vibration modes are listed in Table 2 according to their similar complexes which have been studied [26,33,38–40]. The vibration band around 3467 cm^{-1} is due to overlapping of N—H and O—H stretching. C—H stretching are around 2880 cm^{-1}. The peaks at 1467, 1350, 1280, 1230 and 842 cm^{-1} are related to CH_2 bending, wagging, twisting and rocking vibrations of the film, respectively. Absorption of C═O stretching is at 1650 cm^{-1}. Absorption of C—F, C—S and S—N stretching could be additionally observed in the electrolyte films with LiTFSI. The characteristic peaks of C—*O*—C, C—N, C—S, C—F, S—N, O—H and C═O in every component could be determined in the complex electrolyte films as well, proving that mixture after ball milling is well distributed.

4. Conclusion

Low-cost organic dopants whose molecular weight mainly depended on PAA were synthesized from Poly(allylamine) and L-(+)-tartaric acid with the help of DMAP and EDC and used to change the conductivity of PEO-based electrolytes. An electrolyte

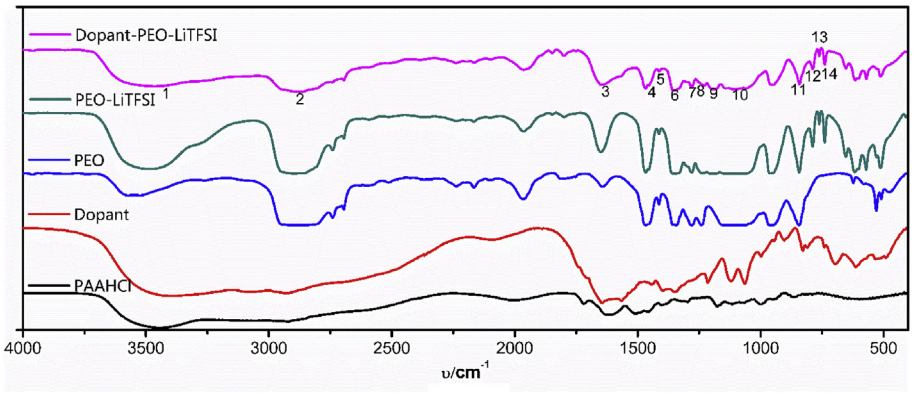

Fig. 5. IR data of dopant-PEO-LiTFSI (5:75:20, w/w), PEO-LiTFSI (75:20, w/w), PEO, high-molecular-weight dopant and PAA·HCl.

Table 2
IR transmittance bands' positions and their assignments in the electrolyte film of dopant-PEO-LiTFSI (5:75:20).

Peak	Wave number/cm^{-1}	Band assignment	Peak	Wave number/cm^{-1}	Band assignment
1	3467	ν N–H, ν O–H	8	1230	ν COC, δ C–H, ν C–N
2	2880	ν C–H	9	1191	ν C–N
3	1650	ν C═O	10	1106	ν COC, ν O–H
4	1467	δ C–H	11	842	δ C–H
5	1413	δ O–H	12	788	ν C–S, ν S–N
6	1350	δ C–H	13	761	ν C–S, δ C–F
7	1280	δ C–H	14	739	ν S–N

whose rate of PEO and lithium salt (LiTFSI) is 75:20 (w/w) was used as a blank sample. Electrolytes with low-molecular-weight dopant shows high room temperature conductivity of over 10^{-4} S cm^{-1} when the rate of dopant and PEO ranged from 4:1 to 0.4:1. But the electrolytes are too weak to separate two electrodes and cannot work stably at high temperature. Less dopant amount resolved the strength and stability problems but no efficient improvement in conductivity was observed. Complexes with high-molecular-weight dopant shows better conductivity (5.4×10^{-6} S cm^{-1}) than electrolyte without dopant (1.3×10^{-6} S cm^{-1}) at room temperature. And sensitive dependence on temperature increasing is also observed constructing to blank sample without dopant (8.1×10^{-4} S cm^{-1} VS 2.6×10^{-4} S cm^{-1} at 80 °C). DSC/TGA and IR measurement were obtained and LSV data of high-molecular-weight dopant doping electrolyte shows lower electrochemical window than electrolyte without dopant. But this film is harder than PEO film and difficult to dissolve, which might be disadvantageous for the manufacture of batteries. Besides, no obvious efficiencies were found when the doping amount changed slightly. Intensive study and application remain further work in the future.

Acknowledgments

This work was financially supported by the National Key R&D Program of China (2016YFB0700600), the Program for Guangdong Introducing Innovative and Entrepreneurial Team (2016ZT06C412), Shenzhen Science and Technology Research Grant (GJHZ20160229122304608).

Appendix A. Supplementary data

Supplementary data to this article can be found online at https://doi.org/10.1016/j.electacta.2018.10.023.

References

[1] A. Arya, A.L. Sharma, Ionics 23 (2017) 497–540.
[2] V. Di Noto, S. Lavina, G.A. Giffin, E. Negro, B. Scrosati, Electrochim. Acta 57 (2011) 4–13.
[3] A.M. Stephan, Eur. Polym. J. 42 (2006) 21–42.
[4] A.M. Stephan, K.S. Nahm, Polymer 47 (2006) 5952–5964.
[5] S. Muench, A. Wild, C. Friebe, B. Haupler, T. Janoschka, U.S. Schubert, Chem. Rev. 116 (2016) 9438–9484.
[6] K. Xu, Chem. Rev. 114 (2014) 11503–11618.
[7] Z. Zhang, Y. Zhao, S. Chen, D. Xie, X. Yao, P. Cui, X. Xu, J. Mater. Chem. A 5 (2017) 16984–16993.
[8] N.S. Choi, Z.H. Chen, S.A. Freunberger, X.L. Ji, Y.K. Sun, K. Amine, G. Yushin, L.F. Nazar, J. Cho, P.G. Bruce, Angew. Chem. Int. Ed. 51 (2012) 9994–10024.
[9] J.B. Goodenough, Y. Kim, Chem. Mater. 22 (2010) 587–603.
[10] M. Osiak, H. Geaney, E. Armstrong, C. O'Dwyer, J. Mater. Chem. A 2 (2014) 9433–9460.
[11] C. Jiang, H.Q. Li, C.L. Wang, Sci. Bull. 62 (2017) 1473–1490.
[12] L. Yang, Z. Wang, Y. Feng, R. Tan, Y. Zuo, R. Gao, Y. Zhao, L. Han, Z. Wang, F. Pan, Adv. Energy Mater. 7 (2017), 1701437.
[13] Z. Wang, R. Tan, H. Wang, L. Yang, J. Hu, H. Chen, F. Pan, Adv. Mater. (2017), 1704436.
[14] R. Gao, R. Tan, L. Han, Y. Zhao, Z. Wang, L. Yang, F. Pan, J. Mater. Chem. A 5 (2017) 5273–5277.
[15] R. Tan, J. Yang, J. Zheng, K. Wang, L. Lin, S. Ji, J. Liu, F. Pan, Nano Energy 16 (2015) 112–121.
[16] D.E. Fenton, J.M. Parker, P.V. Wright, Polymer 14 (1973), 589-589.
[17] J. Zhang, X. Zang, H. Wen, T. Dong, J. Chai, Y. Li, B. Chen, J. Zhao, S. Dong, J. Ma, L. Yue, Z. Liu, X. Guo, G. Cui, L. Chen, J. Mater. Chem. A 5 (2017) 4940–4948.
[18] S. Das, A. Ghosh, AIP Adv. 5 (2015), 027125.
[19] S. Das, A. Ghosh, Electrochim. Acta 171 (2015) 59–65.
[20] A. Ghosh, C.S. Wang, P. Kofinas, J. Electrochem. Soc. 157 (2010) A846–A849.
[21] A. Karmakar, A. Ghosh, J. Appl. Phys. 107 (2010), 104113.
[22] Y.G. Andreev, P.G. Bruce, J. Phys.-Condens. Mat. 13 (2001) 8245–8255.
[23] Z. Gadjourova, Y.G. Andreev, D.P. Tunstall, P.G. Bruce, Nature 412 (2001) 520–523.
[24] F.L. Deng, X.E. Wang, D. He, J. Hu, C.L. Gong, Y.S. Ye, X.L. Xie, Z.G. Xue, J. Membr. Sci. 491 (2015) 82–89.
[25] H.M. Kao, S.W. Chao, P.C. Chang, Macromolecules 39 (2006) 1029–1040.
[26] D. Saikia, C.G. Wu, J. Fang, L.D. Tsai, H.M. Kao, J. Power Sources 269 (2014) 651–660.
[27] F. Croce, S. Sacchetti, B. Scrosati, J. Power Sources 162 (2006) 685–689.
[28] W. Thaharn, T. Bootwicha, D. Soorukram, C. Kuhakarn, S. Prabpai, P. Kongsaeree, P. Tuchinda, V. Reutrakul, M. Pohmakotr, J. Org. Chem. 77 (2012) 8465–8479.
[29] C. Negrell-Guirao, F. Carosio, B. Boutevin, H. Cottet, C. Loubat, J. Polym. Sci., Polym. Phys. Ed. 51 (2013) 1244–1251.
[30] S.A. Babu Naveen, Tetrahedron Lett. 57 (2016) 5801–5807.
[31] G.S. Mahadik, S.A. Knott, L.F. Szczepura, S.R. Hitchcock, Tetrahedron: Asymmetry 20 (2009) 1132–1137.
[32] P. Liu, L. Zhou, C. Yang, H. Xia, Y. He, M. Feng, J. Appl. Polym. Sci. 132 (2015) 41536.
[33] S. Ibrahim, M.M. Yassin, R. Ahmad, M.R. Johan, Ionics 17 (2011) 399–405.
[34] H. Zhang, C. Liu, L. Zheng, F. Xu, W. Feng, H. Li, X. Huang, M. Armand, J. Nie, Z. Zhou, Electrochim. Acta 133 (2014) 529–538.
[35] A. Bartolotta, G. Dimarco, M. Lanza, G. Carini, Nuovo Cimento Della Societa Italiana Di Fisica D-Condensed Matter Atomic Molecular and Chemical Physics Fluids Plasmas Biophysics 16 (1994) 825–830.
[36] W. Preechatiwong, J.M. Schultz, Polymer 37 (1996) 5109–5116.
[37] S. Lascaud, M. Perrier, A. Vallee, S. Besner, J. Prudhomme, M. Armand, Macromolecules 27 (1994) 7469–7477.
[38] B. Laik, L. Legrand, A. Chausse, R. Messina, Electrochim. Acta 44 (1998) 773–780.
[39] S. Abbrent, J. Lindgren, J. Tegenfeldt, A. Wendsjo, Electrochim. Acta 43 (1998) 1185–1191.
[40] H.C. Zhang, X.P. Xuan, J.J. Wang, H.Q. Wang, Solid State Ionics 164 (2003) 73–79.